Chapter 3
The Cell in the Electric Field

Tadej Kotnik, Gorazd Pucihar, and Damijan Miklavčič

Abstract An exposure of a cell to an external electric field results in the induced transmembrane voltage ($\Delta\Psi_m$) that superimposes to the resting voltage. This can have a range of effects, from modification of the activity of voltage-gated channels to membrane electroporation, and accurate knowledge of spatial distribution and time course of $\Delta\Psi_m$ is important for the understanding of these effects. In this chapter, we present the analytical, numerical, and experimental methods of determination of $\Delta\Psi_m$, and combine them with the monitoring of electroporation-induced transmembrane molecular transport (TMT) in Chinese Hamster Ovary (CHO) cells. Potentiometric measurements are performed using di-8-ANEPPS, and TMT is monitored using propidium iodide. In isolated cells, we combine analytical derivation (for spherical cells) and numerical computation of $\Delta\Psi_m$ (for irregularly shaped cells) with potentiometric measurements to show that the latter are accurate and reliable. Monitoring of TMT in these same cells shows that it is confined to the regions with the highest $|\Delta\Psi_m|$. We then review other parameters influencing electroporation of isolated cells, and proceed, through the intermediate case of dense suspensions, to cells in direct contact with each other. We use the scrape-loading test to show that the CHO cells in a monolayer are interconnected, and then study $\Delta\Psi_m$ and TMT in a cluster of four such cells. With low pulse amplitudes, the cluster behaves as one big cell, with $\Delta\Psi_m$ continuous along its outer boundary, reflecting the interconnections. With interconnections inhibited, the cells start to behave as individual entities, with $\Delta\Psi_m$ continuous along the plasma membrane of each cell. With the cluster exposed to porating (higher amplitude) pulses, TMT occurs in the membrane regions for which computations predict the highest $|\Delta\Psi_m|$ if the cells are modeled as insulated, suggesting that the interconnections are blocked by supraphysiological $\Delta\Psi_m$, either directly by voltage gating or indirectly through changes in ionic concentrations caused by electroporation.

Keywords Induced transmembrane voltage • Potentiometric dyes • Electroporation • Molecular transport

Introduction

The spatial distribution of the voltage on the plasma membrane of biological cells has a number of theoretical and experimental implications, such as the activation of voltage-gated membrane channels, cardiac cell stimulation, and plasma membrane electroporation [1–7]. In studies of these phenomena, cells are usually exposed to an external electric field, which induces a voltage across the cell membrane,

T. Kotnik (✉)
Department of Biomedical Engineering, University of Ljubljana, Trzaska 25, 1000 Ljubljana, Slovenia
e-mail: tadej.kotnik@fe.uni-lj.si

S.T. Kee et al. (eds.), *Clinical Aspects of Electroporation*,
DOI 10.1007/978-1-4419-8363-3_3,

termed the induced transmembrane voltage and denoted by $\Delta\Psi_m$ [8, 9]. Unlike the resting transmembrane voltage, which is always present and constant everywhere on the plasma membrane, $\Delta\Psi_m$ only lasts for the duration of the exposure and varies with the position on the membrane. Consequently, it is often important to accurately determine not only its amplitude, but also its spatial distribution.

Many studies imply that plasma membrane electroporation and the resulting molecular flow across the membrane occur in the regions of the membrane exposed to a sufficiently high $\Delta\Psi_m$ [10–14]. Although formation and stabilization of each pore in the membrane is a stochastic process, on the scale of cells and tissues, the effects of membrane electroporation only become detectable at $\Delta\Psi_m$ exceeding a certain "critical" value, $\Delta\Psi_{mC}$ (typically several hundred mV), which treats electroporation as a deterministic process. Thus, for efficient applications of electroporation and understanding of the phenomenon, accurate determination of the distribution of $\Delta\Psi_m$ on the cell membrane is important.

Isolated Cells

Spherical Cells in a Homogeneous Field

In exposures of cells to a direct current (DC) homogeneous electric field, $\Delta\Psi_m$ is determined by solving Laplace's equation. Although biological cells are not perfect spheres, in theoretical treatments they are usually considered as such – a spherical interior (the cytoplasm) surrounded by a concentric spherical shell of uniform thickness (the membrane). For certain types of cells, and particularly for cells in suspensions, this is a reasonable assumption. In the first approximation, the plasma membrane can also be treated as nonconductive. Under these assumptions, the solution of Laplace's equation leads to the formula for $\Delta\Psi_m$ often referred to as the (steady-state) Schwan's equation [15],

$$\Delta\Psi_m = 1.5\, ER\cos\theta, \tag{3.1}$$

where E is the electric field in the region where the cell is situated, R is the cell radius, and θ is the angle measured from the center of the cell with respect to the direction of the field. Thus, $\Delta\Psi_m$ is proportional to the applied electric field and the cell radius. Furthermore, it has extremal values at the points where the field is perpendicular to the membrane, that is, at $\theta=0°$ and $\theta=180°$ (the "poles" of the cell), and in between these poles it varies proportionally to the cosine of θ, as shown in Fig. 3.1b.

$\Delta\Psi_m$, as given by (3.1) is typically established several microseconds after the onset of the electric field. With exposures to a DC field lasting hundreds of microseconds or more, this formula can safely be applied to yield the maximal, steady-state value of the induced transmembrane voltage. To describe the transient behavior during the initial microseconds, one uses the first-order Schwan's equation [8]:

$$\Delta\psi_m = 1.5\, ER\cos\theta\left(1-e^{-t/\tau_m}\right), \tag{3.2}$$

where τ_m is the time constant of the membrane charging and is expressed as:

$$\tau_m = \frac{R\,\varepsilon_m}{2d\,\dfrac{\sigma_i\sigma_e}{\sigma_i+2\sigma_e}+R\sigma_m}, \tag{3.3}$$

with σ_i, σ_m and σ_e as the conductivities of the cytoplasm, cell membrane, and extracellular medium, ε_m the dielectric permittivity of the membrane, d the membrane thickness, and R again the cell radius.

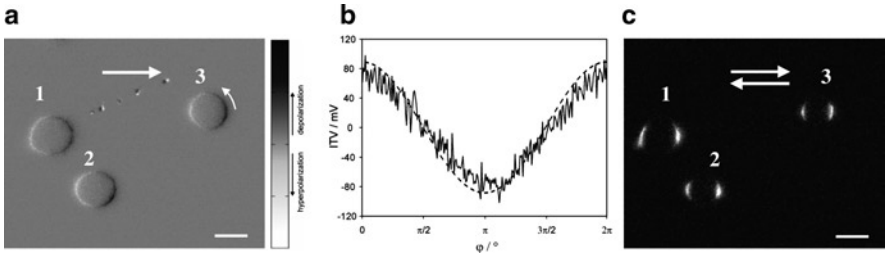

Fig. 3.1 $\Delta\Psi_m$ and electroporation of three spherical CHO cells. (**a**) Changes in fluorescence of di-8-ANEPPS proportional to $\Delta\Psi_m$ caused by a nonporating, 100 V/cm, 50 ms electric pulse. (**b**) Spatial distribution of $\Delta\Psi_m$ as measured on the cell #3 in (**a**) along the path shown by the *arrow* (*solid*), and as predicted by the steady-state Schwan's equation (*dashed*). (**c**) Electroporation obtained on the same cells with an exposure to a 650-V/cm, 750+750 μs bipolar pulse, as visualized by inflow of propidium iodide through the porated membrane regions 100 ms after the exposure. The detected areas of poration imply $\Delta\Psi_{mC} \approx 540$ mV. The bar in (**a**) and (**c**) corresponds to 10 μm

Equations (3.2) and (3.3) are applicable to exposures to sine (alternating current, AC) electric fields with frequencies below 1 MHz and to rectangular electric pulses longer than 1 μs. To determine the time course of $\Delta\Psi_m$ induced by even higher field frequencies or even shorter pulses, the second-order extension of Schwan's equation must be used, in which dielectric permittivities of the cytoplasm and the cell exterior also have to be taken into account [16–18].

An alternative to the analytical derivation of $\Delta\Psi_m$ are the experimental techniques. These include the measurements of $\Delta\Psi_m$ with microelectrodes and with potentiometric fluorescent dyes. The invasive nature of microelectrodes, their low spatial resolution and physical presence, which distorts the electric field, are considerable shortcomings of this approach. In contrast, measurements by means of potentiometric dyes are noninvasive, offer higher spatial resolution, and moreover do not distort the field and thus $\Delta\Psi_m$. As a consequence, during the last decade the potentiometric dyes, such as di-8-ANEPPS [19–22] have become the preferred tool in experimental studies and measurements of $\Delta\Psi_m$.

In Fig. 3.1, the measurements of $\Delta\Psi_m$ on spherical CHO cells are compared to the analytical solution given by (3.1), and a correlation between $\Delta\Psi_m$ and the location of the electroporated membrane regions through which molecular flow occurs is demonstrated. Figure 3.1a, b shows that the measured $\Delta\Psi_m$ correlates well with the theoretical predictions, with the highest values of $\Delta\Psi_m$ found in the membrane regions facing the electrodes (the "poles"). Figure 3.1c shows that the molecular flow through the membrane, and thus membrane electroporation, is confined to these same regions, that is, the areas for which $\Delta\Psi_m > \Delta\Psi_{mC}$.

Nonspherical Geometrically Regular Cells

When suspended, many cells have a shape close to spherical, but for some cell types this is clearly not the case. Among the few generalizations of the cell shape that still allow for analytical derivation of $\Delta\Psi_m$, the most useful are cylinders (e.g., for muscle cells and axons of nerve cells), oblate spheroids (e.g., erythrocytes), and prolate spheroids (e.g., bacilli). To obtain the analogs of Schwan's equation for such cells, one solves Laplace's equation in a suitable coordinate system [23–25]. For a circular cylinder with the axis perpendicular to the field, this yields

$$\Delta\Psi_m = 2ER\cos\theta. \tag{3.4}$$

For an oblate spheroid with the axis of rotational symmetry aligned with the field, we get

$$\Delta\Psi_{\mathrm{m}} = E\frac{R_2^2 - R_1^2}{\left(\frac{R_2^2}{\sqrt{R_2^2 - R_1^2}}\right)\mathrm{arcctg}\left(\frac{R_1}{\sqrt{R_2^2 - R_1^2}}\right) - R_1} \times \frac{R_2\cos\theta}{\sqrt{R_1^2\sin^2\theta + R_2^2\cos^2\theta}} \tag{3.5}$$

and for a prolate spheroid with the axis of rotational symmetry aligned with the field, we get

$$\Delta\Psi_{\mathrm{m}} = E\frac{R_1^2 - R_2^2}{R_1 - \left(\frac{R_2^2}{\sqrt{R_1^2 - R_2^2}}\right)\ln\left(\frac{R_1 + \sqrt{R_1^2 - R_2^2}}{R_2}\right)} \times \frac{R_2\cos\theta}{\sqrt{R_1^2\sin^2\theta + R_2^2\cos^2\theta}} \tag{3.6}$$

where R_1 and R_2 are the radii of the spheroid in the directions parallel and perpendicular to the field, respectively.

A description of a cell is geometrically realistic if the thickness of its membrane is uniform. This is the case if the membrane represents the space between two concentric spheres, but not with two confocal spheroids or ellipsoids. As a result, the thickness of the membrane modeled in spheroidal or ellipsoidal coordinates is necessarily nonuniform. By solving Laplace's equation in these coordinates, we thus obtain the spatial distribution of the electric potential in a nonrealistic setting. However, under the assumption that the membrane conductivity is zero, the induced transmembrane voltage obtained in this manner is still realistic. Namely, the shielding of the cytoplasm is then complete, and hence the electric potential everywhere inside the cytoplasm is constant. Therefore, the geometry of the inner surface of the membrane does not affect the potential distribution outside the cell, which is the same as if the cell were a homogeneous nonconductive body of the same shape. A more rigorous discussion of the validity of this approach can be found in Kotnik and Miklavčič [24].

For nonspherical cells, it is generally more revealing to express $\Delta\Psi_{\mathrm{m}}$ as a function of the arc length along the membrane than as a function of the angle θ (for a sphere, the two quantities are directly proportional). For uniformity, the normalized version of the arc length is used, increasing from 0 to 1 equidistantly along the arc of the membrane.

Irregularly Shaped Cells

Cells in tissues have markedly irregular shapes, deviating considerably from the regular shapes described above. For many such cases, an analytical solution for $\Delta\Psi_{\mathrm{m}}$ cannot be derived. In practice, there are two approaches for obtaining accurate estimates of $\Delta\Psi_{\mathrm{m}}$ on irregularly shaped cells: experimental determination and numerical computation. Experimentally, $\Delta\Psi_{\mathrm{m}}$ can be measured by means of a potentiometric fluorescent dye, as already presented above (see Fig. 3.1). The numerical approach, on the other hand, requires the construction of a model of the cell and subsequent computation of the electric potential inside and outside the cell.

The simplest approach in numerical modeling of an irregularly shaped cell is to compose it from several simple geometrical objects, such as hemispheres and cylinders [26–28]. However, this can only yield a rough approximation of the actual situation, and can thus lead to considerable error. A more realistic three-dimensional model of an irregularly shaped cell can be constructed from a sequence of cross sections of the cell under consideration, as shown in Fig. 3.2 and explained in more detail in Pucihar et al. [29, 30].

In a suitable numerical software package, such as COMSOL Multiphysics, the distribution of the electric potential Ψ in such a model of the cell and its vicinity is then easily computed and the induced transmembrane voltage is determined as the difference between electric potentials on both

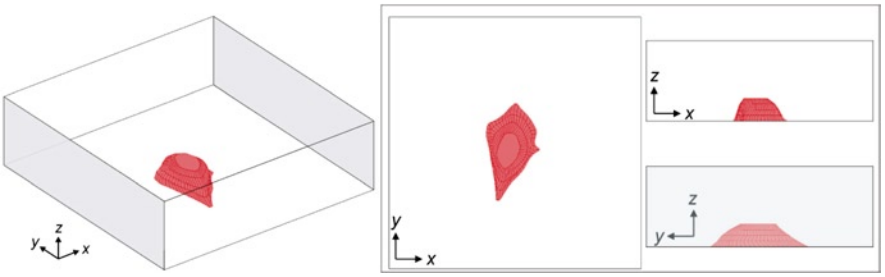

Fig. 3.2 Finite-elements model of a CHO cell attached to a cover glass. The interior of the rectangular block represents the extracellular medium, and the *gray*-shaded faces are the electrodes generating the electric field

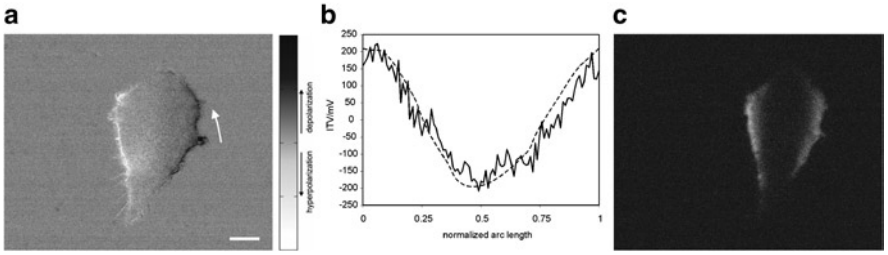

Fig. 3.3 $\Delta\Psi_m$ and electroporation of the CHO cell shown in Fig. 3.2. (**a**) Changes in fluorescence of di-8-ANEPPS proportional to $\Delta\Psi_m$ caused by a nonporating, 100 V/cm, 50 ms electric pulse. (**b**) Spatial distribution of $\Delta\Psi_m$ as measured on a cell in (**a**) along the path shown by the *arrow* (*solid*), and as computed on a model shown in (**a**) (*dashed*). (**c**) Electroporation obtained on the same cell with an exposure to a 1,000 V/cm, 200 μs unipolar pulse, as visualized by inflow of propidium iodide through the porated membrane regions 100 ms after the exposure. The detected areas of poration imply $\Delta\Psi_{mC} \approx 650$ mV. The bar in (**a**) and (**c**) corresponds to 10 μm

sides of the membrane. In analogy to Fig. 3.1, Fig. 3.3a, b demonstrate close correlation between the measured and the numerically computed $\Delta\Psi_m$, while Fig. 3.3c shows that also in irregular cells electroporation occurs in the membrane regions with the highest absolute value of $\Delta\Psi_m$. These regions are generally located in the areas of the membrane closest to (i.e., facing) the electrodes. This is most obvious in cells with pronounced protrusions, where electroporation occurs at their very tips [31].

The results shown in Figs. 3.1 and 3.3 confirm the finding that electroporation is limited to the membrane regions in which the absolute value of $\Delta\Psi_m$ exceeds a certain critical level, $\Delta\Psi_m > \Delta\Psi_{mC}$. With nonspherical shapes, the maximal $\Delta\Psi_m$ attained also depends on the orientation of the cell with respect to the field. Therefore, by exposing the cells to several different orientations of the field, the efficiency of electroporation can be increased significantly, which is also confirmed by experiments [28].

Parameters Influencing Electroporation of Isolated Cells

Pulse Parameters

Electroporation of isolated cells and dilute suspensions in vitro is influenced by both the parameters of the electric pulse(s) and the experimental conditions. Investigations of the role of the amplitude, number, and duration of unipolar rectangular pulses have been the subject of several comprehensive studies [32–36]. These studies show that electroporation only becomes detectable above a certain pulse amplitude, $\Delta\Psi_{mC}$. With further increases in pulse amplitude, the percentage of porated cells

increases, while the percentage of cells surviving the treatment decreases. The average amount of molecules introduced into a cell reaches a peak at some intermediate pulse amplitude. It has also been shown that both poration and cell survival as functions of pulse amplitude vary significantly between various types of cells [37]. Some of the observed differences can be attributed to differences in cell size, but several studies imply that the differences in membrane composition and structure can also play an important role [38, 39].

Experiments show that increasing the number and/or duration of the pulses yields detectable electroporation at a lower minimal pulse amplitude, and that the average amount of molecules introduced into a cell generally increases with an increase of the number of pulses applied [32, 34]. Several studies have demonstrated that for macromolecules such as DNA, electrophoresis plays an important role in the transmembrane transport, and sufficiently long pulse duration is crucial for adequate uptake [33, 34, 40]. Typically, pulse durations for the uptake of smaller molecules are in the range of hundreds of microseconds, while for macromolecules, pulses lasting from several milliseconds to several tens of milliseconds are usually required. Combinations of shorter (electroporating) and longer (electrophoretic) pulses have also been shown to improve the efficiency of gene electrotransfer [41, 42].

At least two studies have focused on a comparison of the efficiency of unipolar and bipolar rectangular pulses in vitro, demonstrating that with bipolar pulses, detectable electroporation is obtained with lower pulse amplitudes, while substantial cell death occurs at similar amplitudes as when unipolar pulses of the same duration are applied [43, 44]. Moreover, contamination of the medium through electrolytical release of metal ions from the electrodes is also lower with bipolar than with unipolar pulses [45].

Unlike the role of the amplitude, number, duration, and polarity of pulses, a hypothetical role of pulse dynamics, or the "pulse shape," has been a subject of relatively few studies. Two reports by the same authors have claimed an improved efficiency of electroporation and gene electrotransfer when a sine wave was superimposed to a rectangular pulse [46, 47]. In another study, rectangular, sine, and triangular waves of the same amplitude were compared, obtaining the most efficient transfection for rectangular, less for sine, and the least for triangular waves [48]. This is in agreement with a later systematic study showing that among the parameters describing the pulse shape, by far the most important for the efficiency of electroporation is the time during which the pulse amplitude exceeds a certain critical value [49]. In another study, it was shown that the efficiency of electroporation is roughly the same for pulse repetition frequencies ranging from 1 Hz (i.e., one pulse per second) up to several kHz, provided that the same total number of pulses is delivered [50].

Experimental Conditions

Electroporation and cell death caused by exposure to high voltage electric pulses also depend on the composition of the extracellular medium. Since electroporation results in substantial exchange of ions between the medium and the cytosol, care must be taken to avoid possible detrimental effects. In particular, in electroporation media, potassium ions are often used instead of the sodium ions of the typical culture media [14, 34, 51]. Also, the calcium ions typically present in culture media should be avoided, as electroporation provides them with a pathway for entering cytosol, leading to supraphysiological intracellular concentrations of Ca^{2+} that can result in cytotoxic effects [52] (as described in Chap. 2).

The electrical conductivity of the extracellular medium also plays a role in electroporation. In media with a conductivity several orders of magnitude below the physiological levels, Schwan's equation as given by (3.1) or (3.2) must be modified by lowering the multiplication factor 1.5 accordingly, as explained in detail in Kotnik et al. [9] and confirmed experimentally in Pucihar et al. [51]. Due to this, in a low-conductivity medium, $\Delta\Psi_m$ induced by a pulse of a given amplitude is

lower than in a physiological medium, and somewhat higher pulse amplitudes must, in general, be applied to obtain the same extent of poration. The decrease in medium conductivity also leads to a lower heating of the cell suspension during the exposure to electroporating pulses [51].

Among the other experimental conditions that influence electroporation are the osmotic pressure and the temperature of the suspension. It was reported that osmotic pressure is not an important factor in transmembrane transport of small molecules, but use of a hypoosmolar buffer during pulsation allows for more efficient uptake of large proteins [53]. With respect to the temperature, postporational incubation at 37°C results in a faster membrane recovery and thus in a higher fraction of cells surviving the treatment. It was also observed that in vitro, the highest uptake of DNA is obtained by incubating the cells before poration at 4°C and after poration at 37°C [54].

Dense Suspensions and Monolayers

In natural situations the cells are rarely isolated, and when sufficiently close to each other, the mutual distortion of the field caused by their proximity cannot be overlooked. Often, the cells are also in direct contact, forming two-dimensional (monolayers attached to the bottom of a dish) or three-dimensional (tissues) structures, and they can even be interconnected.

In dilute cell suspensions, the distance between the cells is much larger than the cell sizes themselves, and the local field outside each cell is practically unaffected by the presence of other cells. Thus, for cells representing less than 1% of the suspension volume (for a spherical cell with a radius of 10 μm, this means up to two million cells/mL), the deviation of the induced transmembrane voltage, $\Delta\Psi_m$, from the prediction given by (3.1) is negligible. However, for larger volume fractions occupied by the cells, the distortion of the local field around each cell by the adjacent cells becomes more pronounced. As the volume fraction occupied by the cells increases beyond 10% and approaches 50%, the spatial distribution of $\Delta\Psi_m$ starts to deviate significantly from that given by (3.1), as the factor 1.5 gradually decreases towards 1, and the distribution also starts to diverge from the ideal cosine shape, as shown in detail in Susil et al. [55], Pavlin et al. [56], and Pucihar et al. [57]. Due to the lower $\Delta\Psi_m$, the efficiency of electroporation with the same pulse parameters is typically lower in dense suspensions than in dilute ones [57].

For even larger volume fractions, the cells come into direct contact, and the electrical properties of the suspension start to resemble that of a tissue, but only to a certain extent. Namely, cells can form specific structures, such as layers, and moreover in tissues they can also be directly electrically coupled, for example, through gap junctions. The amplitude and the spatial distribution of $\Delta\Psi_m$ on these cells can differ considerably from $\Delta\Psi_m$ observed on single isolated cells. This is because dense cell packing shields the cells electrically to some extent, and intercellular pathways can connect adjacent cells electrically. Due to the nature of the tissue structure, it is difficult to observe these effects experimentally in individual tissue cells. As a more feasible alternative, we can study clusters of cells growing in monolayers, which present a simple model for examining the behavior of cells in tissues. As in tissues, cells in clusters also have complex geometrical shapes, are densely packed, and are often connected with intercellular pathways. Thus, the only significant deviation is their two-dimensional arrangement, as opposed to typically three-dimensional cellular structures of tissues.

Intracellular pathways, also termed gap junctions, are small protein channels that allow for the exchange of ions between neighboring cells. The opened or closed state of the gap junctions renders the cells electrically connected or electrically insulated, respectively, and in this manner it can affect $\Delta\Psi_m$ and electroporation considerably.

Figure 3.4 shows that CHO cells form gap junctions allowing for exchange of ions and smaller molecules between the cells, and that these gap junctions are inhibited (blocked) effectively using oleamide. Figures 3.5 and 3.6 show a numerical model and an experiment performed on a cluster of four such cells attached to a cover glass.

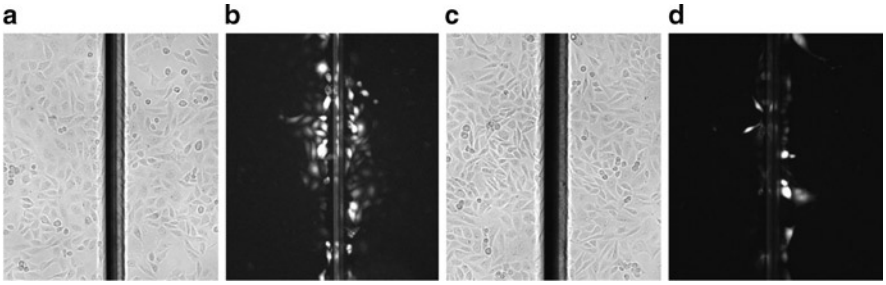

Fig. 3.4 Scrape loading test with 1 mM Lucifer Yellow performed on CHO cells. (**a**) Phase contrast image of the cells scraped with a needle (*black vertical* in the *middle*). (**b**) Fluorescence of the cells 5 min later. The dye entered the damaged cells and quickly diffused into the neigboring, undamaged cells. (**c**) Same as (**a**), but with the cells preincubated for 45 min with 200 μM oleamide, a gap junction inhibitor. (**d**) Fluorescence 5 min later. The dye only entered the cells directly damaged by scraping

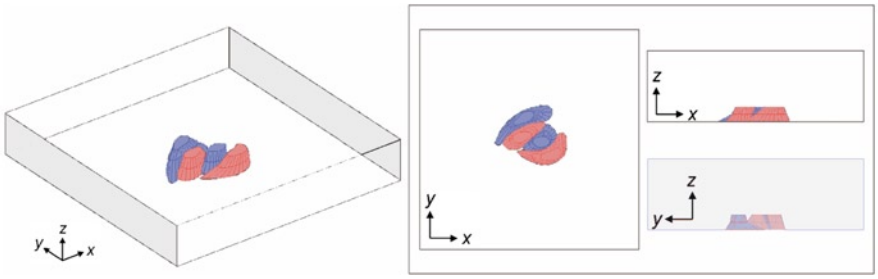

Fig. 3.5 Finite-elements model of a cluster of CHO cells forming a monolayer cluster attached to a cover glass. By changing the electrical conductivity of the membrane regions forming contacts between the cells, cells in clusters can be modeled as either electrically interconnected or electrically insulated

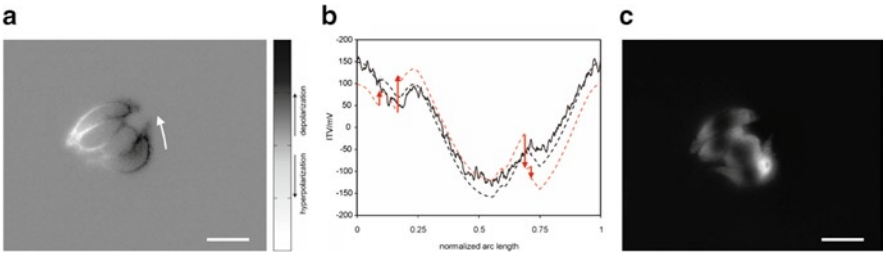

Fig. 3.6 $\Delta\Psi_m$ and electroporation of a cluster of the four attached CHO cells shown in Fig. 3.5. (**a**) Changes in fluorescence of di-8-ANEPPS proportional to $\Delta\Psi_m$ caused by a nonporating, 75 V/cm, 50 ms electric pulse. (**b**) Spatial distribution of $\Delta\Psi_m$ as measured on the cluster in (**a**) along its outer boundary as shown by the *arrow* (*solid*), and numerically computed $\Delta\Psi_m$ for electrically interconnected (*dashed black*) and electrically insulated cells (*dashed gray*). The *arrows* show the discontinuities of $\Delta\Psi_m$ along the outer cluster boundary with insulated cells. (**c**) Electroporation obtained on the same cluster with an exposure to a 1,000 V/cm, 750 + 750 μs bipolar pulse, as visualized by inflow of propidium iodide through the porated membrane regions 500 ms after the exposure. The bar in (**a**) and (**c**) corresponds to 20 μm

With nonelectroporating pulses (lower amplitude, longer duration) and without inhibition of the gap junctions, $\Delta\Psi_m$ induced on the membranes of the cells was continuous when traced along the outer boundary of the cluster (Fig. 3.6b, solid curve). This correlates well with the numerically computed $\Delta\Psi_m$ for the case of electrically interconnected cells (Fig. 3.6b, dashed black). In other

words, the cluster behaved as if it was one big cell, reflecting the interconnections of the cells by gap junctions.

Applying the same pulse parameters, but with the gap junctions inhibited, the cells started behaving as individual entities (i.e., as electrically insulated), so that $\Delta\Psi_m$ was continuous along the plasma membrane of each individual cell, yet discontinuous when traced along the outer boundary of the cluster (Fig. 3.6b, dashed gray, with discontinuities marked by arrows).

When the cluster was exposed to electroporating pulses (higher amplitude, shorter duration), however, the molecular transport occurred in the membrane regions for which numerical computations predicted the highest $\Delta\Psi_m$ if the cells were modeled as insulated. The results were unaffected by the presence or absence of oleamide, suggesting that with $\Delta\Psi_m$ substantially above the physiological levels, the gap junctions can also be blocked by another mechanism, perhaps directly by voltage gating, or indirectly as a consequence of changes in ionic concentrations caused by electroporation. The ongoing investigations should cast additional light on these observations.

Within clusters of cells, in a similar fashion to isolated nonspherical cells, the efficiency of electroporation depends on the orientation of the field with respect to the cells. If a single pulse is used for electroporation, the appropriate field orientation with respect to the cell should be chosen for optimal effects. For applications in which the aim is to achieve electroporation, but the size of the porated area is unimportant, it is advisable to orient the field along the larger dimension of the cell, for example, so that the longest protrusions face the electrodes. For such an orientation, a moderate external field will induce $\Delta\Psi_m > \Delta\Psi_{mC}$ only at the very ends of these protrusions. In contrast, if the aim is to maximize the size of the porated area, the field should generally be oriented perpendicularly to the larger dimension of the cell (see e.g., Fig. 3.3). With several pulses applied, an improved efficiency can be obtained by changing the field orientation between consecutive pulses. As this approach renders a higher electroporated area of the membranes, it allows the use of a somewhat lower pulse amplitude, resulting in reduced loss of cell viability [58, 59].

In addition to the variability of cell shapes, a recent study suggests that also $\Delta\Psi_{mC}$ can vary considerably even between cells of the same type [60]. As a consequence, numerical modeling can be useful for analyzing the spatial distribution of $\Delta\Psi_m$ on the membranes of the cells under consideration when planning an efficient electroporation protocol, but the location and size of the porated membrane regions can only be estimated [30].

References

1. Bedlack RS, Wei M, Fox SH, et al. Distinct electric potentials in soma and neurite membranes. Neuron. 1994;13:1187–93.
2. Cheng DKL, Tung L, Sobie EA. Nonuniform responses of transmembrane potential during electric field stimulation of single cardiac cells. Am J Physiol. 1999;277:H351–62.
3. Neumann E, Kakorin S, Toensing K. Fundamentals of electroporative delivery of drugs and genes. Bioelectrochem Bioenerg. 1999;48:3–16.
4. Teissié J, Eynard N, Gabriel B, et al. Electropermeabilization of cell membranes. Adv Drug Deliv Rev. 1999;35:3–19.
5. Burnett P, Robertson JK, Palmer JM, et al. Fluorescence imaging of electrically stimulated cells. J Biomol Screen. 2003;8:660–7.
6. Sharma V, Tung L. Ionic currents involved in shock-induced nonlinear changes in transmembrane potential responses of single cardiac cells. Pflugers Arch. 2004;449:248–56.
7. Huang CJ, Harootunian A, Maher MP, et al. Characterization of voltage-gated sodium-channel blockers by electrical stimulation and fluorescence detection of membrane potential. Nat Biotechnol. 2006;24:439–46.
8. Pauly H, Schwan HP. Über die Impedanz einer Suspension von kugelformigen Teilchen mit einer Schale. Z Naturforsch B. 1959;14:125–31.
9. Kotnik T, Bobanović F, Miklavčič D. Sensitivity of transmembrane voltage induced by applied electric fields – a theoretical analysis. Bioelectrochem Bioenerg. 1997;43:285–91.

10. Hibino M, Shigemori M, Itoh H, et al. Membrane conductance of an electroporated cell analyzed by submicrosecond imaging of transmembrane potential. Biophys J. 1991;59:209–20.
11. Hibino M, Itoh H, Kinosita Jr K. Time courses of cell electroporation as revealed by submicrosecond imaging of transmembrane potential. Biophys J. 1993;64:1789–800.
12. Tekle E, Astumian RD, Chock PB. Selective and asymmetric molecular-transport across electroporated cell-membranes. Proc Natl Acad Sci USA. 1994;91:11512–6.
13. Gabriel B, Teissié J. Direct observation in the millisecond time range of fluorescent molecule asymmetrical interaction with the electropermeabilized cell membrane. Biophys J. 1997;73:2630–7.
14. Gabriel B, Teissié J. Time courses of mammalian cell electropermeabilization observed by millisecond imaging of membrane property changes during the pulse. Biophys J. 1999;76:2158–65.
15. Schwan HP. Electrical properties of tissue and cell suspensions. Adv Biol Med Phys. 1957;5:147–209.
16. Grosse C, Schwan HP. Cellular membrane potentials induced by alternating fields. Biophys J. 1992;63: 1632–42.
17. Kotnik T, Miklavčič D, Slivnik T. Time course of transmembrane voltage induced by time-varying electric fields – a method for theoretical analysis and its application. Bioelectrochem Bioenerg. 1998;45:3–16.
18. Kotnik T, Miklavčič D. Second-order model of membrane electric field induced by alternating external electric fields. IEEE Trans Biomed Eng. 2000;47:1074–81.
19. Fluhler E, Burnham VG, Loew LM. Spectra, membrane binding, and potentiometric responses of new charge shift probes. Biochemistry. 1985;24:5749–55.
20. Gross D, Loew LM, Webb W. Optical imaging of cell membrane potential changes induced by applied electric fields. Biophys J. 1986;50:339–48.
21. Loew LM. Voltage sensitive dyes: measurement of membrane potentials induced by DC and AC electric fields. Bioelectromagnetics. 1992;Suppl 1:179–89.
22. Pucihar G, Kotnik T, Miklavčič D. Measuring the induced membrane voltage with di-8-ANEPPS. J Visual Exp 2009;33:1659.
23. Bernhard J, Pauly H. Generation of potential differences across membranes of ellipsoidal cells in an alternating electrical field. Biophysik. 1973;10:89–98.
24. Kotnik T, Miklavčič D. Analytical description of transmembrane voltage induced by electric fields on spheroidal cells. Biophys J. 2000;79:670–9.
25. Gimsa J, Wachner D. Analytical description of the transmembrane voltage induced on arbitrarily oriented ellipsoidal and cylindrical cells. Biophys J. 2001;81:1888–96.
26. Fear EC, Stuchly MA. Modeling assemblies of biological cells exposed to electric fields. IEEE Trans Biomed Eng. 1998;45:1259–71.
27. Buitenweg JR, Rutten WL, Marani E. Geometry-based finite-element modeling of the electrical contact between a cultured neuron and a microelectrode. IEEE Trans Biomed Eng. 2003;50:501–9.
28. Valič B, Golzio M, Pavlin M, et al. Effect of electric field induced transmembrane potential on spheroidal cells: theory and experiment. Eur Biophys J. 2003;32:519–28.
29. Pucihar G, Kotnik T, Valič B, et al. Numerical determination of transmembrane voltage induced on irregularly shaped cells. Ann Biomed Eng. 2006;34:642–52.
30. Pucihar G, Miklavčič D, Kotnik T. A time-dependent numerical model of transmembrane voltage inducement and electroporation of irregularly shaped cells. IEEE Trans Biomed Eng. 2009;56:1491–501.
31. Teruel MN, Meyer T. Electroporation-induced formation of individual calcium entry sites in the cell body and processes of adherent cells. Biophys J. 1997;73:1785–96.
32. Rols MP, Teissié J. Electropermeabilization of mammalian cells. Quantitative analysis of the phenomenon. Biophys J. 1990;58:1089–98.
33. Wolf H, Rols MP, Boldt E, et al. Control by pulse duration of electric-field mediated gene transfer in mammalian cells. Biophys J. 1994;66:524–31.
34. Rols MP, Teissié J. Electropermeabilization of mammalian cells to macromolecules: control by pulse duration. Biophys J. 1998;75:1415–23.
35. Canatella PJ, Karr JF, Petros JA, et al. Quantitative study of electroporation-mediated molecular uptake and cell viability. Biophys J. 2001;80:755–64.
36. Maček-Lebar A, Miklavčič D. Cell electropermeabilization to small molecules *in vitro*: control by pulse parameters. Radiol Oncol. 2001;35:193–202.
37. Čemažar M, Jarm T, Miklavčič D, et al. Effect of electric-field intensity on electropermeabilization and electrosensitivity of various tumor-cell lines *in vitro*. Electro Magnetobiol. 1998;17:261–70.
38. Troiano GC, Tung L, Sharma V, et al. The reduction in electroporation voltages by the addition of a surfactant to planar lipid bilayers. Biophys J. 1998;75:880–8.
39. Kandušer M, Fošnarič M, Šentjurc M, et al. Effect of surfactant polyoxyethylene glycol ($C_{12}E_8$) on electroporation of cell line DC3F. Colloid Surface A. 2003;214:205–17.

40. Sukharev SI, Klenchin VA, Serov SM, et al. Electroporation and electrophoretic DNA transfer into cells. Biophys J. 1992;63:1320–7.
41. Satkauskas S, André F, Bureau MF, et al. Electrophoretic component of electric pulses determines the efficacy of *in vivo* DNA electrotransfer. Human Gene Ther. 2005;16:1194–201.
42. Kandušer M, Miklavčič D, Pavlin M. Mechanisms involved in gene electrotransfer using high- and low-voltage pulses – an *in vitro* study. Bioelectrochemistry. 2009;74:265–71.
43. Tekle E, Astumian RD, Chock PB. Electroporation by using bipolar oscillating electric field: an improved method for DNA transfection of NIH 3T3 cells. Proc Natl Acad Sci USA. 1994;88:4230–4.
44. Kotnik T, Mir LM, Flisar K, et al. Cell membrane electropermeabilization by symmetrical bipolar rectangular pulses. Part I. Increased efficiency of permabilization. Bioelectro-chemistry. 2001;54:83–90.
45. Kotnik T, Miklavčič D, Mir LM. Cell membrane electropermeabilization by symmetrical bipolar rectangular pulses: Part II. Reduced electrolytic contamination. Bioelectrochemistry. 2001;54:91–5.
46. Chang DC. Cell poration and cell fusion using an oscillating electric field. Biophys J. 1989;56:641–52.
47. Chang DC, Gao PQ, Maxwell BL. High efficiency gene transfection by electroporation using a radio-frequency electric field. Biochim Biophys Acta. 1991;1092:153–60.
48. Xie TD, Tsong TY. Study of mechanisms of electric field-induced DNA transfection. II. Transfection by low-amplitude, low-frequency alternating electric fields. Biophys J. 1990;58:897–903.
49. Kotnik T, Pucihar G, Reberšek M, et al. Role of pulse shape in cell membrane electropermeabilization. Biochim Biophys Acta. 2003;1614:193–200.
50. Pucihar G, Mir LM, Miklavčič D. The effect of pulse repetition frequency on the uptake into electropermeabilized cells *in vitro* with possible applications in electrochemotherapy. Bioelectrochemistry. 2002;57:167–72.
51. Pucihar G, Kotnik T, Kandušer M, et al. The influence of medium conductivity on electropermeabilization and survival of cells *in vitro*. Bioelectrochemistry. 2001;54:107–15.
52. Nicotera C, Bellomo G, Orrenius S. Calcium-mediated mechanisms in chemically induced cell death. Annu Rev Pharmacol Toxicol. 1992;32:449–70.
53. Golzio M, Mora MP, Raynaud C, et al. Control by osmotic pressure of voltage-induced permeabilization and gene transfer in mammalian cells. Biophys J. 1998;74:3015–22.
54. Rols MP, Delteil C, Serin G, et al. Temperature effects on electrotransfection of mammalian cells. Nucleic Acids Res. 1994;22:540.
55. Susil R, Šemrov D, Miklavčič D. Electric field induced transmembrane potential depends on cell density and organization. Electro Magnetobiol. 1998;17:391–9.
56. Pavlin M, Pavšelj N, Miklavčič D. Dependence of induced transmembrane potential on cell density, arrangement, and cell position inside a cell system. IEEE Trans Biomed Eng. 2002;49:605–12.
57. Pucihar G, Kotnik T, Teissié J, et al. Electroporation of dense cell suspensions. Eur Biophys J. 2007;36: 173–85.
58. Reberšek M, Faurie C, Kandušer M, et al. Electroporator with automatic change of electric field direction improves gene electrotransfer *in vitro*. Biomed Eng Online. 2007;6(25):1–11.
59. Trontelj K, Reberšek M, Kandušer M, et al. Optimization of bulk cell electrofusion *in vitro* for production of human–mouse heterohybridoma cells. Bioelectrochemistry. 2008;74:124–9.
60. Towhidi L, Kotnik T, Pucihar G, et al. Variability of the minimal transmembrane voltage resulting in detectable membrane electroporation. Electromagn Biol Med. 2008;27:372–85.